water

MDPI

Article

Iron-Loaded Pomegranate Peel as a Bio-Adsorbent for Phosphate Removal

Naoufal Bellahsen [1], Balázs Kakuk [2], Sándor Beszédes [3], Zoltán Bagi [2], Nóra Halyag [4], Tamás Gyulavári [5], Szabolcs Kertész [3], Ahmed El Amarti [6], Etelka Tombácz [7] and Cecilia Hodúr [3,*]

1 Faculty of Science and Informatics, Doctoral School of Environmental Science, University of Szeged, Moszkvai krt. 9, 6725 Szeged, Hungary; naoufal.bel@hotmail.com
2 Department of Biotechnology, University of Szeged, Közép fasor 52, 6726 Szeged, Hungary; kakuk.balazs@med.u-szeged.hu (B.K.); bagiz@brc.hu (Z.B.)
3 Department of Process Engineering, Faculty of Engineering, University of Szeged, Moszkvai krt. 9, 6725 Szeged, Hungary; beszedes@mk.u-szeged.hu (S.B.); kertesz@mk.u-szeged.hu (S.K.)
4 Institute of Raw Materials Preparation and Environmental Processing, Faculty of Earth Science & Engineering, University of Miskolc, Egyetemváros, 3515 Miskolc, Hungary; ejtpnora@uni-miskolc.hu
5 Department of Applied and Environmental Chemistry, University of Szeged, Rerrich B. ter 1, 6720 Szeged, Hungary; gyulavarit@chem.u-szeged.hu
6 Department of Chemistry, Faculty of Science of Tetouan, University of Abdelmalek Esaadi, Avenue de Sebta, Mhannech II, Tetouan 93002, Morocco; ahmed-elamarti@hotmail.com
7 Soós Water Technology Research and Development Center, University of Pannonia, 8200 Nagykanizsa, Hungary; tombacz.etelka@sooswrc.hu
* Correspondence: hodur@mk.u-szeged.hu; Tel.: +36-62-546-500

check for updates

Citation: Bellahsen, N.; Kakuk, B.; Beszédes, S.; Bagi, Z.; Halyag, N.; Gyulavári, T.; Kertész, S.; Amarti, A.E.; Tombácz, E.; Hodúr, C. Iron-Loaded Pomegranate Peel as a Bio-Adsorbent for Phosphate Removal. *Water* **2021**, *13*, 2709. https://doi.org/10.3390/w13192709

Academic Editor: Laura Bulgariu

Received: 28 July 2021
Accepted: 28 September 2021
Published: 30 September 2021

Abstract: This study investigated the adsorption of phosphate from aqueous solutions using pomegranate peel (PP) as a bio-adsorbent. For this purpose, PP was activated via saponification using sodium hydroxide (NaOH) followed by cationization using iron chloride ($FeCl_3$). The iron-loaded PP (IL-PP) was characterized using zeta potential measurement, scanning electron microscopy, and Fourier transform infrared analysis. The batch adsorption method was followed to determine the equilibrium time and effect of pH on the adsorption process. The full factorial design methodology was used to analyze the effects of influencing parameters and their interactions. The effective removal of phosphate up to 90% was achieved within 60 min, at pH 9 and 25 °C temperature using a 150 mg dose of IL-PP. A non-linear method was used for the modeling of isotherm and kinetics. The results showed that the kinetics is best fitted to the Elovich model (R^2 = 0.97), which assumes the dominance of the chemisorption mechanism, whereas the isotherm obeys both Langmuir (R^2 = 0.98) and Freundlich (R^2 = 0.94) models with a maximum phosphate uptake of 49.12 mg·g^{-1}. Investigation of thermodynamic parameters indicated the spontaneity and endothermic nature of the process. These results introduce IL-PP as an efficient bio-adsorbent of phosphate.

Keywords: adsorption; bio-adsorbent; phosphate removal; pomegranate peel; recycling

1. Introduction

Excess release of phosphorus is the main culprit for the eutrophication of freshwater and marine ecosystems [1]. Phosphorus is a nonrenewable and irreplaceable element for plant growth, and its role is crucial in agricultural production [2]. The accelerated growth in food demand has also increased the demand for phosphate fertilizers, which has placed stress on phosphate rock sources and is exhausting existing deposits [3]. The phosphate mining industry is also facing serious challenges regarding water availability for the mining process and a decrease in the quality of phosphate rocks [4]. Thus, the recovery of phosphate from wastewater is highly required to sustain the global food supply, preserve water resources, and protect the environment. Several biological, physical, and chemical methods exist for phosphate removal and recovery from aqueous solutions [5,6]. Among

them, adsorption technologies are the most advantageous because of their simplicity, cost-effectiveness, and wide availability of existing and potential adsorbents that can potentially be directly applied to soil as fertilizer when loaded with phosphate [3,7].

Expanding agricultural activities in addition to irresponsible food production and consumption has resulted in more than 1.3 billion tons of agricultural and food waste deposited annually according to the Food and Agriculture Organization of the United Nations (FAO), which has had several environmental, financial, and social implications [8,9]. Although reducing this waste is one of the Sustainable Development Goals for 2030, efforts remain insufficient because more awareness and radical changes are needed in consumer attitudes and economic policies of countries. Different approaches have been considered for the revalorization of this biomass waste to gain environmental, financial, and social benefits, such as livestock feed, bioenergy production, bioactive compound recovery, food industry, and soil fertilization [10,11]. One approach has been to convert biomass waste into bio-adsorbents for pollutant removal and recovery [12–16]. However, the biomass waste must be activated to develop desirable physicochemical properties for phosphate uptake [17].

Pomegranate peel (PP) is a widely abundant biomass waste because of the huge production of the pomegranate fruit. Approximately 1.5 million tons of PP is estimated to be produced per year [16], which is a major environmental concern for producer countries (e.g., India, Iran, Turkey, the United States, China, Spain, and Morocco) [18,19]. To mitigate this problem, various revalorization methods have been introduced, such as the production of valuable compounds for essential oils [20,21], food additives [22], and medicinal products [23], as well as energy and value-added products such as bioethanol and biogas [24,25]. PP is increasingly being used as a bio-adsorbent for heavy metals, dyes, and other contaminants [9,26–42]. The present study investigated the efficiency of activated PP at phosphate removal from an aqueous solution.

2. Materials and Methods

2.1. The Stock Solution

The stock solution of phosphate (1000 mg·L^{-1}) was prepared by dissolving $Na_2HPO_4 \cdot 2H_2O$ in deionized water, which was then diluted to the desired concentrations using distilled water. The adjustment of pH values of the phosphate solutions was done using hydrochloric acid (HCl) and sodium hydroxide (NaOH) solutions. All chemicals used in this study were of analytical reagent grade.

2.2. Preparation and Activation of PP

PP was activated using an iron loading method similar to that of Nguyen et al. [43] for improving the PO_4^{3-} retention ability. First, PP was collected, cut into small pieces, and washed with distilled water several times until the washing solution became clear. It was oven-dried at 105 °C for 2 h and then ground to the desired particle size (<250 µm). The first step of the activation method was the base treatment or saponification, where 40 g of PP was stirred for 24 h with 1 L of a NaOH solution (0.05 M) at room temperature and then washed carefully with distilled water until the pH of washing solution became neutral. The saponification step aimed to improve the cationic exchange capacity of PP and promote the incorporation of iron ions (Fe^{3+}) on its surface. The second step was the iron loading, where the saponified PP was stirred with 500 mL of an iron chloride ($FeCl_3$) solution (0.25 M) at room temperature for 24 h. Finally, the iron-loaded PP (IL-PP) was carefully washed with distilled water again and oven-dried at 105 °C for 8 h, and then, it was mechanically milled with a planetary ball mill to the desired particle size (<250 µm) before use in the adsorption experiments.

2.3. Characterization of IL-PP

The zeta potentials of PP and IL-PP were measured using 10 mg suspensions mixed in bottles containing 30 mL of sodium chloride (NaCl) and disodium hydrogen phosphate

(Na_2HPO_4) solutions at different concentrations and pH values. After mixing, the equilibrium pH of the samples was measured and adjusted. Then, the zeta potential was measured with a Nano ZS apparatus (Malvern, Worcestershire, UK) using electrophoretic light scattering. All samples were prepared in triplicate, and the average of the measurements was used for data analysis.

Scanning electron microscopy (SEM) was also used to image the microstructures of PP and IL-PP and compare their surface morphologies. Samples were analyzed using a Hitachi S-4700 type II scanning electron microscope. A cold field emission gun and 10 kV acceleration voltage were applied to respectively produce and accelerate the electron beam. Micrographs were recorded by collecting secondary electrons with an Everhart–Thornley detector.

Fourier transform infrared (FTIR) spectra of PP and IL-PP were used to observe the functional groups present on their surface and assess the occurred changes after the activation of PP and the adsorption of phosphate (PO_4^{3-}) by IL-PP. The spectra were recorded with a BIO-RAD Digilab Division FTS-65A/896 FTIR spectrophotometer having a 4 cm^{-1} resolution in the middle infrared range of 4000–400 cm^{-1}. Each spectrum was scanned 256 times. In addition to the spectra of each sample, single-reflection diamond attenuated total reflection accessory measurements were taken using the diffuse reflection technique and an angle of incidence of 45°. The software Omnic 7.3 was used for FTIR data collection.

2.4. Batch Adsorption

The batch adsorption method was used to determine the equilibrium time and effect of pH on PO_4^{3-} adsorption by IL-PP. For this purpose, 50 mL of Na_2HPO_4 solution (PO_4-P concentration of 40 $mg{\cdot}L^{-1}$) was stirred at 150 rpm with different IL-PP doses (100 and 150 mg) doses and pH values (from 3 to 9) at a constant temperature of 25 °C. To identify the most important factors affecting the removal of PO_4^{3-} by IL-PP, 2^3 factorial design (three factors each, at two levels) with the Minitab 19 software was used. This technique allows the analysis of several factors simultaneously within a reduced total number of experiments [44]. The initial PO_4-P concentration (40 $mg{\cdot}L^{-1}$), contact time (60 min), and stirring speed (150 rpm) were kept constant, and the three factors of the pH, adsorbent dose, and solution temperature were varied at two levels, as shown in Table 1.

Table 1. Levels of parameters used in the factorial design for PO_4^{3-} removal by IL-PP.

Parameter	Coded Symbol	Low Level (−1)	High Level (+1)
pH	A	3	9
Adsorbent dose (mg)	B	100	150
Temperature (°C)	C	25	45

PO_4-P concentration was determined by Spectrophotometer Spectroquant Nova 60 (Merck, Germany) after filtering samples through 0.45 µm microporous membrane filters.

The PO_4^{3-} removal rate was calculated using Equation (1):

$$\text{Removal } \% = \frac{C_i - C_f}{C_i} \cdot 100 \tag{1}$$

where C_i ($mg{\cdot}L^{-1}$) and C_f ($mg{\cdot}L^{-1}$) are the initial and final PO_4-P concentrations, respectively.

The adsorbed amount of PO_4-P was calculated using Equation (2):

$$q_e \left(mg{\cdot}g^{-1}\right) = (C_i - C_e)\frac{V}{M} \tag{2}$$

where C_i ($mg{\cdot}L^{-1}$) and C_e ($mg{\cdot}L^{-1}$) are the initial and equilibrium concentrations, respectively, of PO_4-P in the solution; V (L) is the solution volume; and M (g) is the mass of the adsorbent.

The isotherm of PO_4^{3-} adsorption by IL-PP was studied through a series of batch adsorption experiments at a stable temperature using different doses of IL-PP and a constant initial PO_4-P concentration. Factorial design experiments were performed to identify and optimize the adsorption kinetics. To determine the isotherm and kinetic models that adequately describe PO_4^{3-} adsorption by IL-PP, isotherm and kinetics data were fitted to existing mathematical models by a nonlinear method using the Solver add-in command in Microsoft Excel [45]. The best fitting kinetic and isotherm models were selected mainly based on the value of the nonlinear correlation coefficient (R^2). However, the chi-square (χ^2) statistics helped confirm this selection. A value of χ^2 close to 0 meant that the selected model fit the experimental data well, whereas a high value of χ^2 indicated that the model was inappropriate [46]. R^2 and χ^2 were calculated using Equations (3) and (4), respectively:

$$R^2 = \frac{\sum\left(q_{e,cal} - q_{e,mean}\right)^2}{\sum\left(q_{e,cal} - q_{e,mean}\right)^2 + \sum\left(q_{e,cal} - q_{e,exp}\right)^2} \quad (3)$$

$$\chi^2 = \sum \frac{\left(q_{e,exp} - q_{e,cal}\right)^2}{q_{e,cal}} \quad (4)$$

where $q_{e,exp}$ ($mg \cdot g^{-1}$) is the amount of PO_4-P uptake at equilibrium obtained from Equation (2), $q_{e,cal}$ ($mg \cdot g^{-1}$) is the amount of PO_4-P uptake calculated from the model using the Solver add-in command, and $q_{e,mean}$ ($mg \cdot g^{-1}$) is the mean of the $q_{e,exp}$ values.

To study the thermodynamics of PO_4^{3-} adsorption by IL-PP, parameters such as the standard Gibbs free energy change (ΔG), standard enthalpy change (ΔH), and standard entropy change (ΔS) were determined using Equations (5) and (6):

$$\Delta G = -R\,T\,\ln K_d \quad (5)$$

$$\mathrm{Ln}K_d = \frac{\Delta H^\circ}{R\,T} + \frac{\Delta S^\circ}{R} \quad (6)$$

where T is the absolute temperature in kelvins and R is the gas constant (8.314 J mol^{-1} K^{-1}). K_d is the distribution coefficient for the adsorption and was obtained by plotting ln (q_e/C_e) against C_e and extrapolating to zero Ce. Then, the obtained value was multiplied by 1000 as proposed by Milonjić [47].

3. Results and Discussion

3.1. Characterization Results

3.1.1. Zeta Potential

Determining the zeta potential of the electric double layer surrounding the adsorbent surface at various solutions with different pH values and similar ionic strength (IS) is important because it provides insights into the adsorbent surface chemistry and possible interactions with the adsorbate [48]. Figure 1a shows that in the NaCl solution (IS = 10), IL-PP showed a positive zeta potential over the entire pH range considered in this study: from +5.8 mV at pH 3 to +16.1 mV at pH 9. By contrast, PP showed negative values: from −26.7 mV at pH 3 to −30.6 mV at pH 9. These results indicate that the PP surface became positively charged after the incorporation of Fe^{3+}. The zeta potential of IL-PP in the Na_2HPO_4 solution (IS = 10) decreased from +11.3 to −31.8 mV when the pH was increased from 3 to 9, and the isoelectric point can be interpolated at pH 5.4. This means that the IL-PP surface had an excess negative charge at pH > 5.4 and an excess positive charge at pH < 5.4. The decrease in surface charge is due to the neutralization of positive functional groups present on the IL-PP surface (mainly Fe^{3+}) by PO_4^{3-}. However, in the NaCl solution, Cl^- could not neutralize the IL-PP surface, so the IL-PP surface had a high affinity toward PO_4^{3-} through a specific adsorption mechanism rather than a simple electrostatic attraction. Figure 1b shows that the zeta potential of IL-PP decreased when

the Na_2HPO_4 concentration was increased. The compression of the diffuse layer, which caused more PO_4^{3-} anions to attach to this layer could be the reason for this behavior [49].

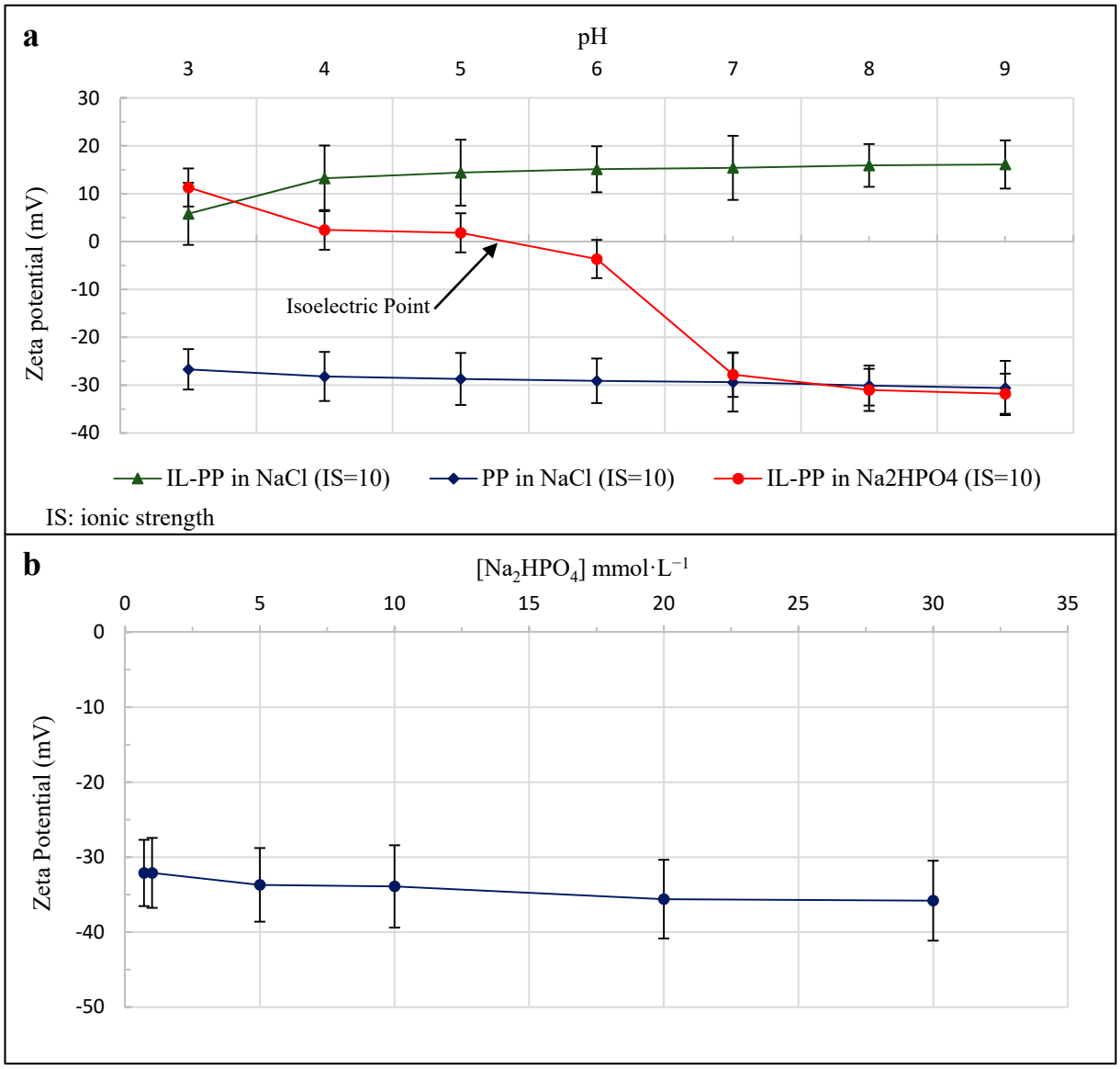

Figure 1. Zeta potentials of PP and IL-PP in NaCl and Na_2HPO_4 solutions as functions of pH (**a**) and IL-PP as a function of the Na_2HPO_4 concentration (**b**).

3.1.2. SEM Results

Figure 2 shows SEM micrographs of PP (a) and IL-PP (b) at 50,000× magnification. The PP surface was relatively smooth and flat, but IL-PP had a much rougher surface with a coarser texture, which proves that Fe^{3+} was incorporated. This modification of the morphology made the surface irregular and thus more suitable for PO_4^{3-} uptake [50].

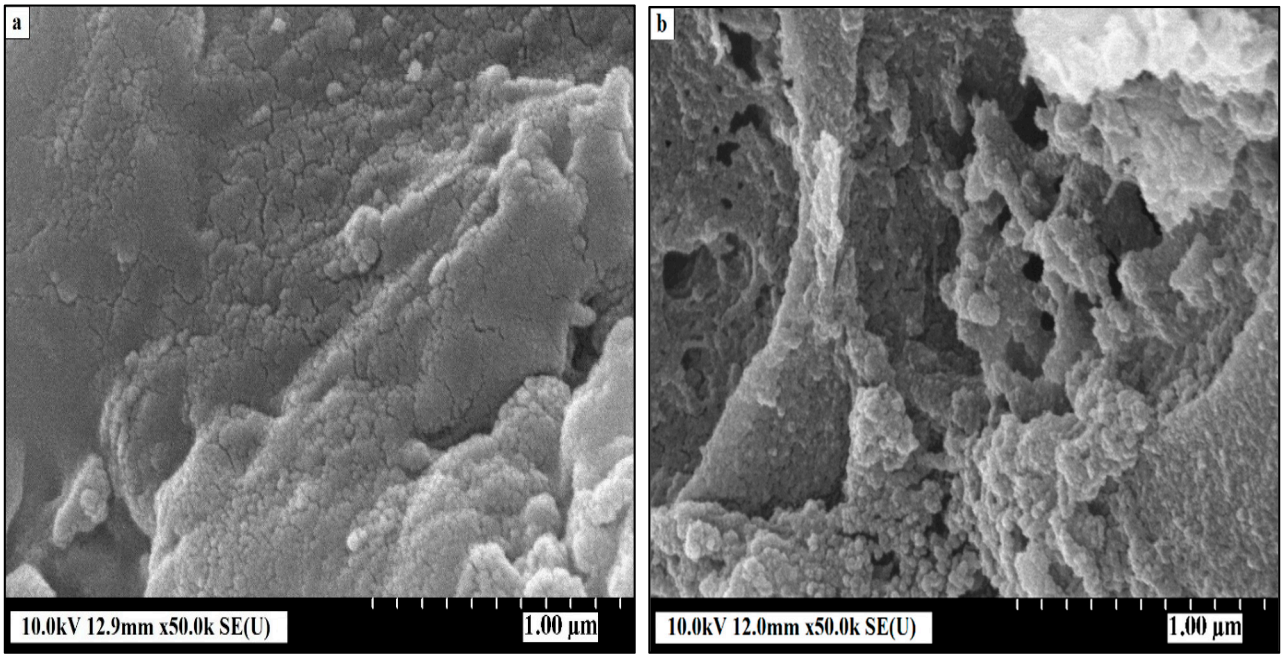

Figure 2. SEM images of PP (**a**) and IL-PP (**b**).

3.1.3. FTIR Analysis

Figure 3 shows the FTIR spectra of PP and IL-PP before and after PO_4^{3-} adsorption. Table 2 presents the results of the analysis carried out to identify the functional groups present on their surfaces and understand the possible interactions responsible for the incorporation of Fe^{3+} onto the surface of PP and for the adsorption of PO_4^{3-} by IL-PP. The observed bands in the PP surface agree with similar FTIR studies on functional groups present in PP [31,51]. However, the IL-PP spectra showed important changes characterized mainly by the appearance of a new peak at 801 cm^{-1}, which can be assigned to the Fe–OH band [52,53], and the disappearance of several bands at 1719, 1442, 1223, 876, and 747 cm^{-1}. These variations confirm the incorporation of Fe^{3+} on the PP surface. The IL-PP spectra after PO_4^{3-} adsorption revealed the appearance of a new peak at 1601 cm^{-1}, which can be attributed to the bending vibration of Fe–P and, therefore, confirms PO_4^{3-} adsorption by IL-PP [54].

Table 2. FTIR analysis of PP and IL-PP before and after PO_4^{3-} adsorption.

Adsorption Band (cm^{-1})			Assignment
PP	IL-PP	IL-PP after PO_4^{3-} Adsorption	
3323	3306	3327	–OH and N–H
2931	2918	2924	C–H, $–CH_3$, or $–CH_2$
1719	–	–	C=O and C–C
1615	1617	–	C=C, C=O, or N–H
–	–	1601	Fe-P
1442	–	–	–OH
1320	1313	1318	C–H, $–CH_3$, or $–CH_2$
1223	–	–	O–H
1031	1030	–	C-O and C-O–C
876	–	–	O–H, C=O, and O–H
–	801	–	Fe–OH
747	–	–	C–N

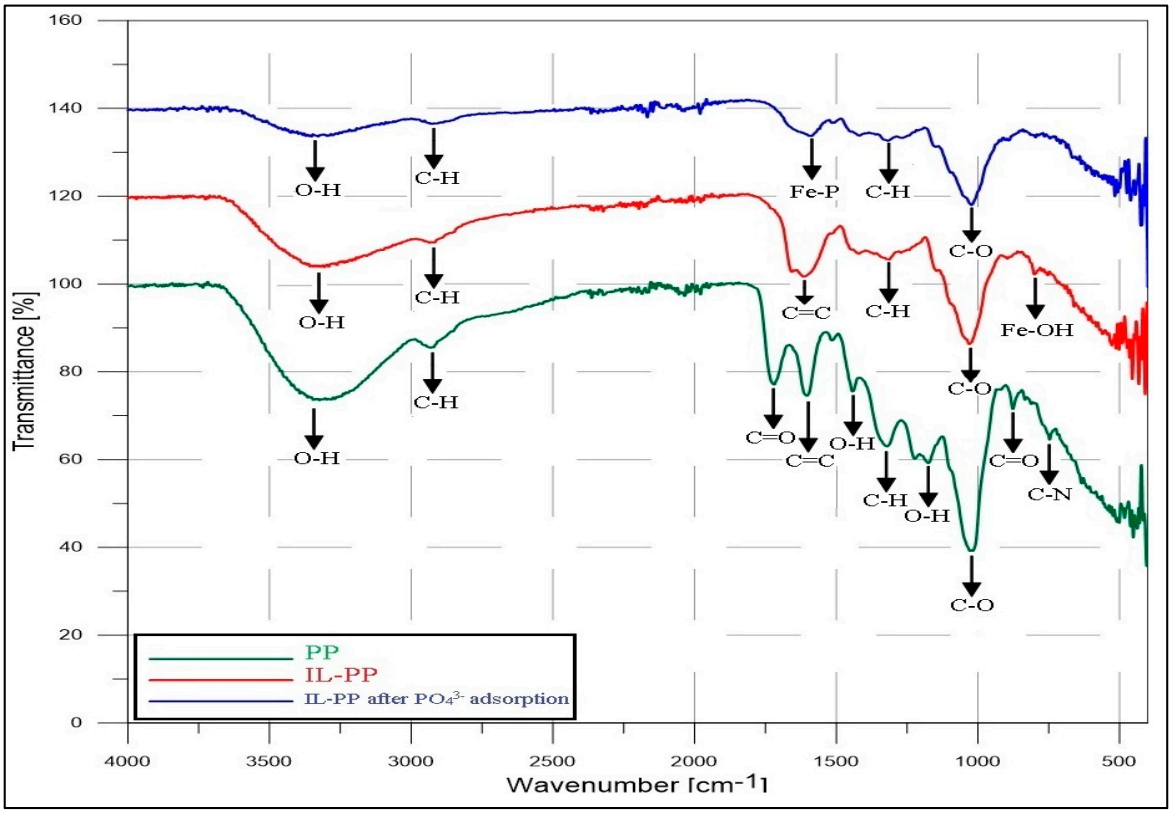

Figure 3. FTIR spectra of PP and IL-PP before and after PO_4^{3-} adsorption.

3.2. Batch Adsorption Results

3.2.1. Effect of pH

The pH is a critical parameter in the adsorption process because it affects the chemistry of the solution and the stability of functional groups present on the adsorbent surface, which controls the adsorbent–adsorbate interaction [55]. Depending on the solution pH, PO_4^{3-} can exist in four species: H_3PO_4 (pH~2.15), $H_2PO_4^-$ (2.15 < pH < 7.20), HPO_4^{2-} (7.20 < pH < 12.33), and PO_4^{3-} (pH~12.33) [56]. Figure 4 shows that PO_4^{3-} removal by 100 mg of IL-PP increased from 43.5% to 64.25% when the pH was increased from 3 to 9. This is because there is just one possible interaction between $H_2PO_4^-$ and Fe^{3+}, which is monodentate/mononuclear. However, there are three different possible interactions between HPO_4^{2-} and Fe^{3+}: monodentate/mononuclear, bidentate/mononuclear, and monodentate/binuclear [57]. This led to the high PO_4^{3-} removal by IL-PP. These results are in agreement with the decrease in the zeta potential of the IL-PP surface in the Na_2HPO_4 solution when the pH was increased, which indicates that more PO_4^{3-} ions were attached to this surface. For each sample, the equilibrium pH value was lower than the initial pH value, which indicates that large quantities of hydrogen ions were produced by Fe^{3+} hydrolysis and reduced the equilibrium pH [58].

3.2.2. Determination of the Equilibrium Time

Figure 5 shows the equilibrium time for PO_4^{3-} removal by IL-PP, which was studied using two different doses of IL-PP (100 and 150 mg) and fixed values for the PO_4-P concentration (40 mg·L^{-1}), pH (9), and temperature (25 °C). Within the first 2 min, rapid PO_4^{3-} uptake took place with removal rates of 51% and 76.5% for 100 and 150 mg, respectively, of IL-PP. This fast uptake is due to the presence of a large number of active sites to which a large amount of PO_4^{3-} anions could attach. Afterward, due to the saturation of available active sites, the removal rate decreased and equilibrium approached [13]. The equilibrium state for PO_4^{3-} removal was reached within 60 min. Removal rates of 64.25% and 90% were achieved with 100 and 150 mg, respectively, of IL-PP.

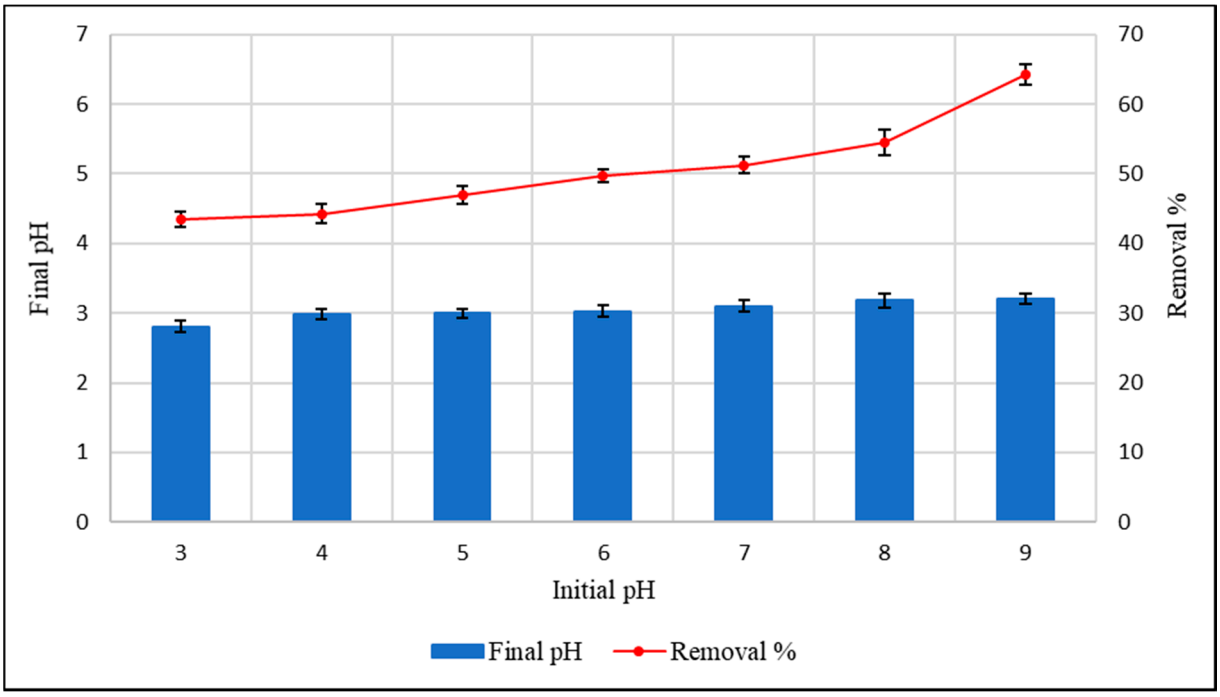

Figure 4. Effect of pH on PO_4^{3-} removal by IL-PP (PO_4-P concentration: 40 mg·L^{-1}, adsorbent dose: 100 mg, temperature: 25 °C, stirring speed: 150 rpm).

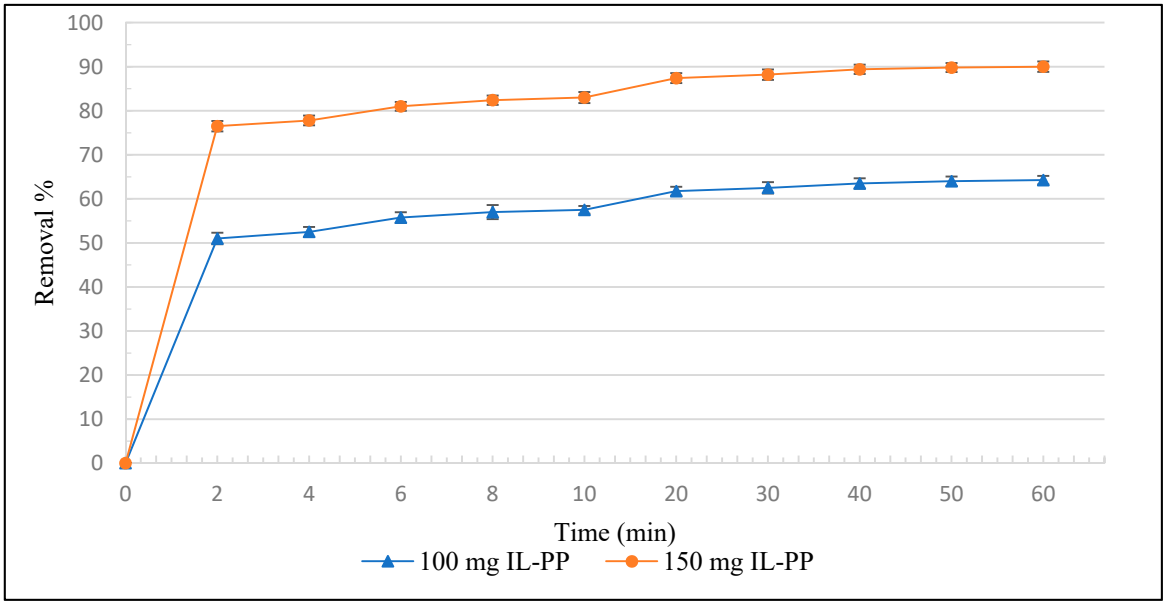

Figure 5. Effect of contact time on PO_4^{3-} removal by IL-PP (PO4-P concentration: 40 mg·L^{-1}, pH: 9, temperature: 25 °C, stirring speed: 150 rpm).

3.2.3. Factorial Design

The factorial design methodology was used to determine the importance of the three factors (pH, adsorbent dose, and temperature) and their interactions on PO_4^{3-} removal by IL-PP. Factorial design plots such as plots for the main effects and interactions, Pareto chart, and normal plot for the standardized effects describe the interactive relation between the factors and their levels [59]. This technique investigates all possible combinations and verifies the accuracy of the obtained mathematical model through the analysis of variance (ANOVA) to achieve optimum removal of PO_4^{3-}. Table 3 and Figure 6 present the results

of the factorial design experiments and average values for the response variable (PO_4^{3-} removal rate) based on the high and low levels of the studied parameters.

Table 3. Design matrix and results of the 2^3 factorial design for PO_4^{3-} removal by IL-PP.

Run	pH (A)	Adsorbent Dose (B)	Temperature (°C)	Removal Rate (%)	Standard Deviation
1	1	−1	−1	61.08	2.74
2	−1	1	1	87.5	1.32
3	1	1	−1	90	2.5
4	−1	1	−1	81.66	2.93
5	−1	−1	−1	41.16	3.35
6	1	1	1	90.75	1.75
7	1	−1	1	68.25	2.61
8	−1	−1	1	49.16	2.56

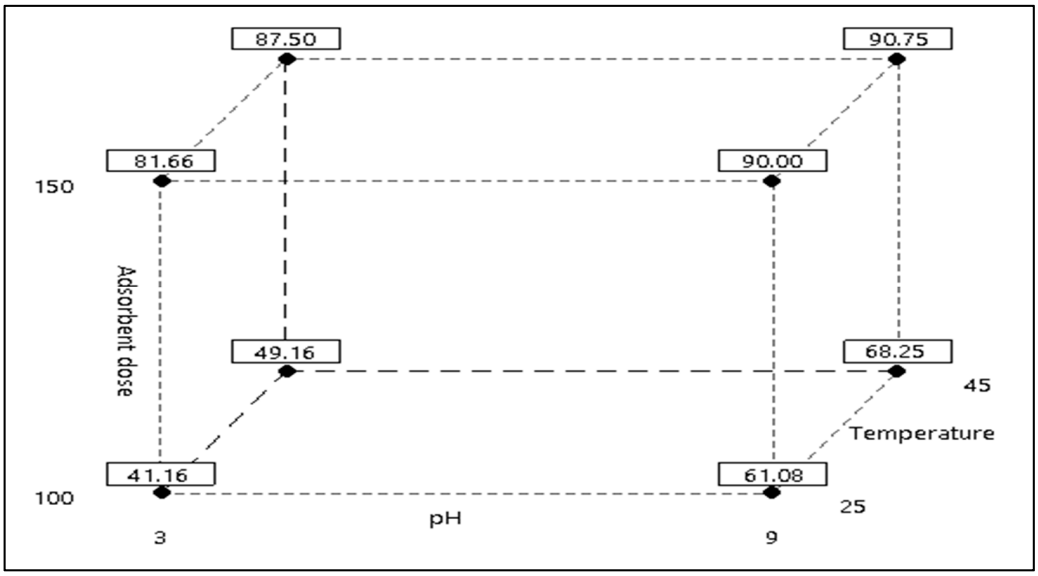

Figure 6. Cube plots for PO_4^{3-} removal by IL-PP.

Table 4 presents the main and interaction effects, model coefficients, standard deviation of each coefficient, standard errors, Fisher test value (F-value), and probability value (*p*-value). All of the main effects (pH, adsorbent dosage, temperature, and two- and three-way interactions) were significant at a 5% probability level ($p < 0.05$). Furthermore, the adjusted square correlation coefficient R^2 (adj) had a value of 99.99%, which indicates that the presented model perfectly fit the statistical model [44].

Table 4. Estimated effects and coefficients for PO_4^{3-} removal by IL-PP.

Term	Effect	Coef	SE Coef	T-Value	*p*-Value	VIF
Constant		71.1979	0.0276	2583.39	0.000	
pH	12.6458	6.3229	0.0276	229.42	0.000	1.00
Adsorbent dose	32.5625	16.2813	0.0276	229.42	0.000	1.00
Temperature	5.4375	2.7188	0.0276	590.76	0.000	1.00
pH × Adsorbent dose	−6.8542	−3.4271	0.0276	−124.35	0.000	1.00
pH × Temperature	−1.4792	−0.7396	0.0276	−26.84	0.000	1.00
Adsorbent dose × Temperature	−2.1458	−1.0729	0.0276	−38.93	0.000	1.00
pH × Adsorbent dose × Temperature	−1.0625	−0.5312	0.0276	−19.28	0.000	1.00
S	0.135015					
R^2	100.00%					
R^2 (Adj)	99.99%					
R^2 (Pred)	99.99%					

Model for PO_4^{3-} removal by IL-PP can be expressed using Equation (7):

$$PO_4^{-3}\text{ removal }\% = -72.00 + 5.583\text{ A} + 0.92688\text{ B} + 0.4250\text{ C} - 0.0209\text{A}\cdot\text{B} + 0.06389\text{A}\cdot\text{C} - 0.000042\text{ B}\cdot\text{C} - 0.000708\text{ A}\cdot\text{B}\cdot\text{C} \quad (7)$$

where A is the pH, B is the adsorbent dose, and C is the temperature; AB, AC, and BC represent the two-way interactions; and ABC represents the three-way interaction.

Equation (7) describes how the experimental parameters and their interactions influence the response variable and thus can be used to predict responses for given levels of each parameter [60]. Positive values in the equation indicate that the PO_4^{3-} removal increases when this effect increases. By contrast, negative values indicate that the removal rate decreases when this effect increases [59]. An analysis of variance was performed to investigate the significance of parameters affecting PO_4^{3-} removal to ensure the accuracy of the model. Table 5 presents the sum of the squares used to estimate the effect of factors, the F-ratio (i.e., the ratio of individual mean square effects to the mean square error) and the *p*-value (i.e., the level of significance leading to the rejection of the null hypothesis). The results showed that the main effects of each factor, their two-way interactions, and the three-way interaction were statistically significant at $p < 0.05$.

Table 5. Analysis of variance for PO_4^{3-} removal by IL-PP.

Source	DF	Adj SS	Adj MS	F-Value	*p*-Value
Model	7	7828.21	1118.32	61,347.57	0.000
Linear	3	7498.80	2499.60	137,120.90	0.000
pH	1	959.50	959.50	52,635.57	0.000
Adsorbent dose	1	6361.90	6361.90	348,995.57	0.000
Temperature	1	177.40	177.40	9731.57	0.000
Two-way interactions	3	322.63	107.54	5899.57	0.000
pH × Adsorbent dose	1	281.88	281.88	15,463.00	0.000
pH × temperature	1	13.13	13.13	720.14	0.000
Adsorbent dose × temperature	1	27.63	27.63	1515.57	0.000
Three-way interaction	1	6.77	6.77	371.57	0.000
pH × adsorbent dose × temperature	1	6.77	6.77	371.57	0.000
Error	16	0.29	0.02		
Total	23	7828.50			

Figure 7 shows the main effects of each parameter on PO_4^{3-} removal by IL-PP by giving the deviations between high and low levels of each parameter, which can help with identifying which parameters affect the response variable the most. A larger deviation is synonymous with a large effect [61]. The adsorbent dose appears to have the greatest effect on PO_4^{3-} removal by IL-PP, which is followed by pH and then temperature, which had an almost negligible effect.

Figure 8 plots the interactions of the studied parameters. If the interaction lines are not parallel, this implies that the interaction has a strong effect, whereas parallel interaction lines indicate a weak effect [62]. The most important interaction for PO_4^{3-} removal by IL-PP appears to be pH*adsorbent dose, which is followed by adsorbent dose*temperature. The least important interaction was pH*temperature, which had almost parallel interaction lines.

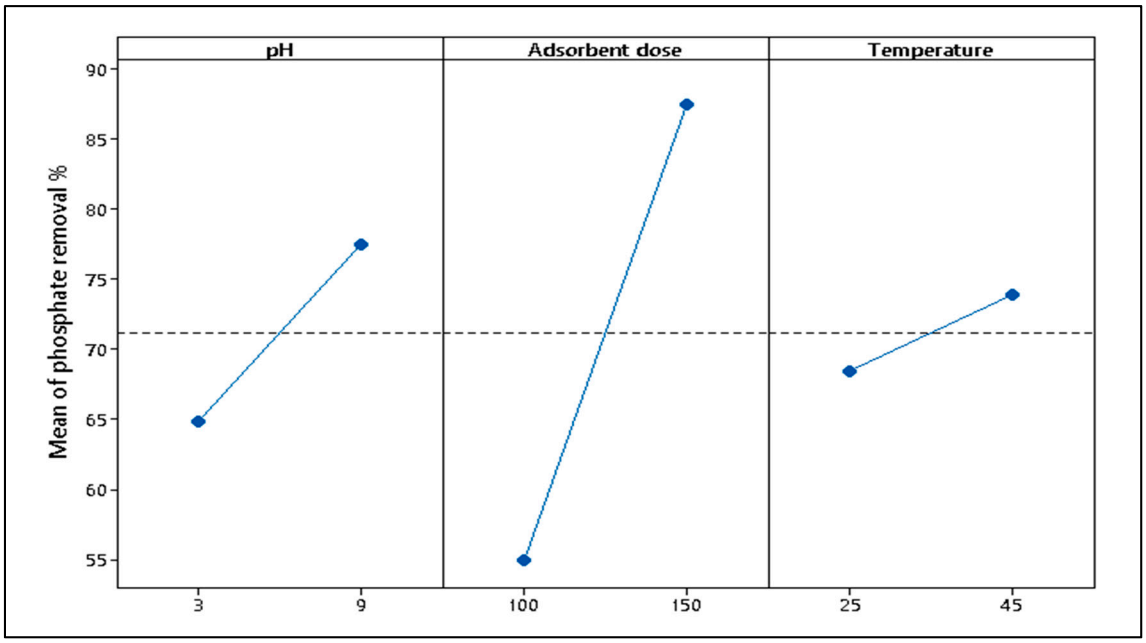

Figure 7. Plots for the main effects of PO_4^{3-} removal by IL-PP.

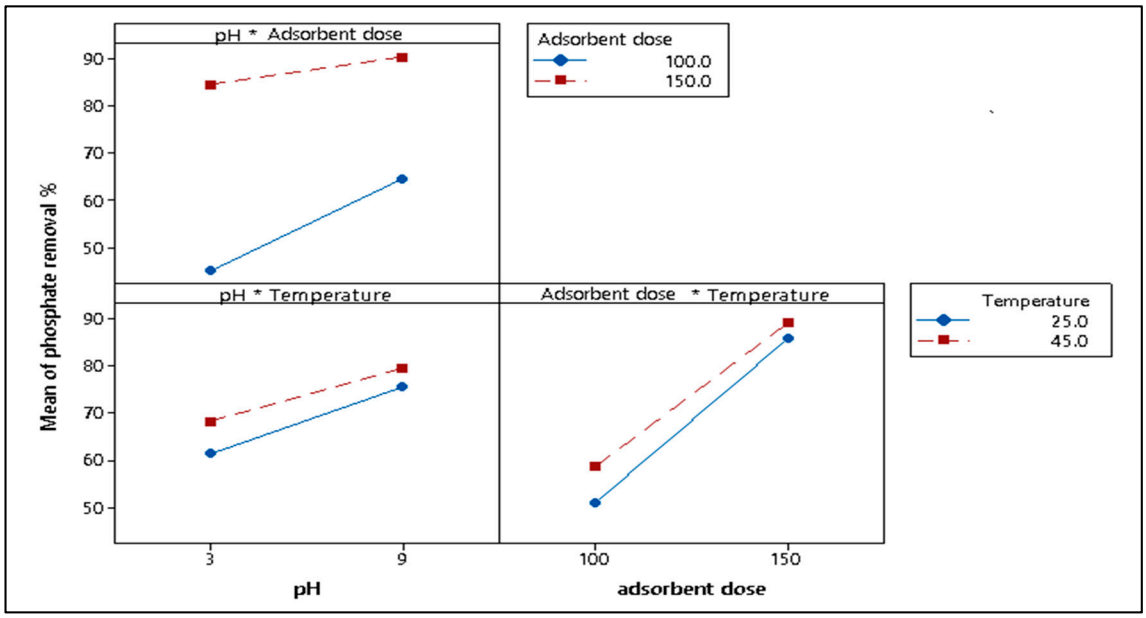

Figure 8. Plots for the interactions due to PO_4^{3-} removal by IL-PP (%).

A Pareto chart is helpful for observing the relative importance of the main effects of factors and their interactions. This chart can be used to evaluate the significance of effects on the basis of how much they exceed the reference line [63]. Figure 9 shows that all parameters and their interactions had a significant effect because their values exceeded that of the reference line (2.1, in red).

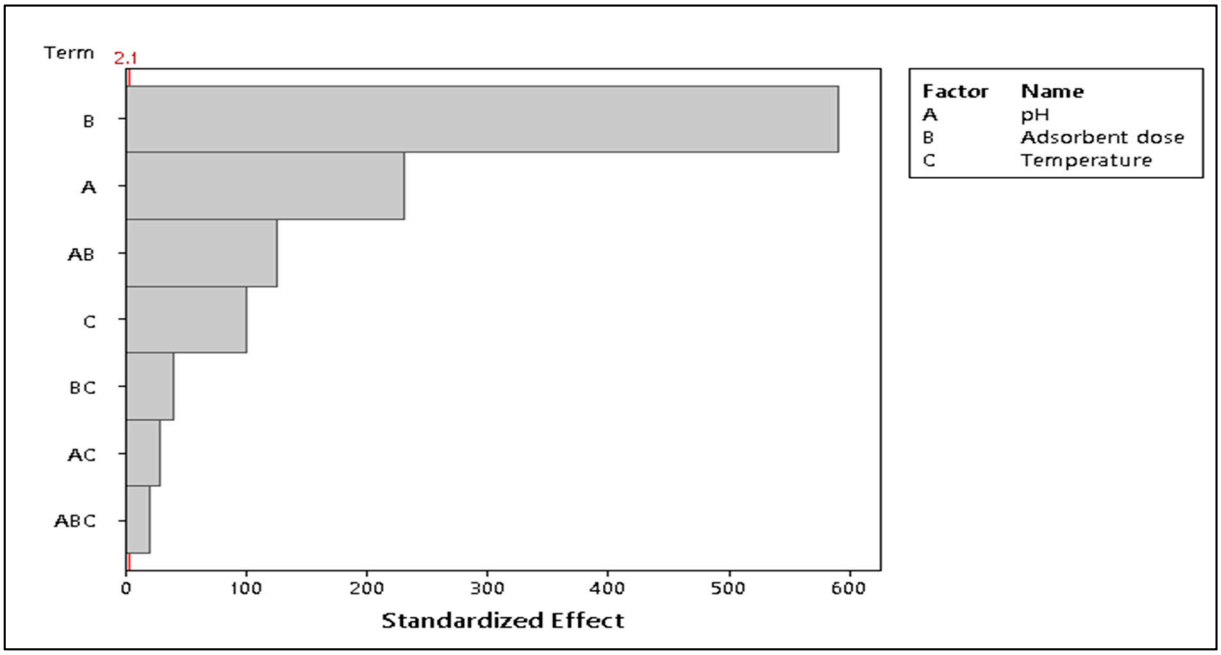

Figure 9. Pareto chart for the standardized effects of PO_4^{3-} removal by IL-PP.

Figure 10 shows a normal plot of the standardized effects, which was used to identify the "real" effects. Each point on this plot was attributed to an effect. Points far from the reference line likely represent the greatest effect and vice versa [63]. The adsorbent dose (B) had the greatest effect since its point was farthest from the reference line (in red),which followed by pH (A) and their interaction (AB). The adsorbent dose (B) and pH (A) had positive effects because their points are on the right side of the line, whereas their interaction (AB) had a negative effect because it is on the left side [44]. The significance of the effects of the parameters and their interactions can be ordered as follows: B > A > AB > C > BC > AC > ABC.

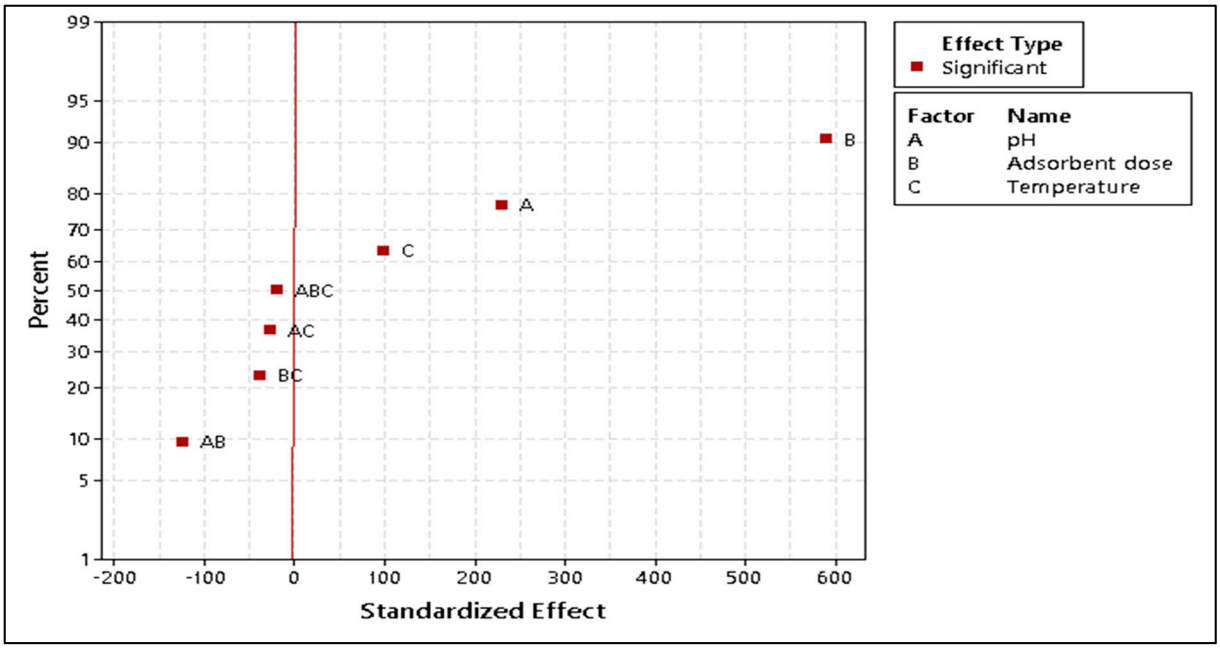

Figure 10. Normal plot for the standardized effects of PO_4^{3-} removal by IL-PP.

3.3. Process Modeling

3.3.1. Kinetics

Adsorption kinetics represents the progress of the adsorption process over time. Determining the adsorption kinetics helps with identifying the governing mass transfer mechanism and the characteristic mass transfer parameters [55]. To identify the mechanisms and potential rate-controlling step for PO_4^{3-} adsorption by IL-PP, four kinetic models were examined: the pseudo-first-order, pseudo-second-order, Elovich equation, and intraparticle diffusion models. Equations (8)–(11) respectively present the nonlinear forms of these models:

$$q_t = q_e\left(1 - e^{-k_1 t}\right) \tag{8}$$

$$q_t = \frac{{q_e}^2 k_2 t}{1 + k_2 q_e t} \tag{9}$$

$$q_t = \frac{1}{\beta}\ln\left(1 + \alpha\beta t\right) \tag{10}$$

$$q_t = k3\sqrt{t} + C \tag{11}$$

where q_e and q_t are the amounts of PO_4-P adsorbed at equilibrium and at time t, respectively. k_1 ($L{\cdot}min^{-1}$), k_2 ($g{\cdot}mg^{-1}{\cdot}min^{-1}$), α ($mg{\cdot}g^{-1}{\cdot}min^{-1}$), and k_3 ($mg{\cdot}g^{-1}{\cdot}min^{-1}$) are constants of the pseudo-first-order, pseudo-second-order, Elovich equation, and intraparticle diffusion models, respectively. β ($mg{\cdot}g^{-1}$) is the desorption constant during any one experiment, and C is a constant describing the thickness of the boundary layer.

Table 6 gives the adsorption constant of each model as well as the calculated and experimental values of q_e ($q_{e,cal}$ and $q_{e,exp}$, respectively), R^2, and χ^2.

Table 6. Kinetic models and parameters of PO_4^{3-} adsorption by IL-PP.

Kinetic Model	$q_{e,cal}$ ($mg{\cdot}g^{-1}$)	Parameters	R^2	χ^2	$q_{e,exp}$ ($mg{\cdot}g^{-1}$)
Pseudo-first-order	11.44	k_1 = 1.01 ($L{\cdot}min^{-1}$)	0.39	0.22	12
Pseudo-second-order	11.85	k_2 = 0.19 ($g{\cdot}mg^{-1}{\cdot}min^{-1}$)	0.83	0.05	
Elovich equation	12.11	α ($\times 10^6$) = 11.88 ($mg{\cdot}g^{-1}{\cdot}min^{-1}$) β = 1.72 ($mg{\cdot}g^{-1}$)	0.97	0.007	
Intraparticle diffusion	12.22	k_3 = 0.28 ($mg{\cdot}g^{-1}{\cdot}min^{-1}$) C = 10.04	0.91	0.03	

On the basis of the R^2 and χ^2 values and comparison between $q_{e,cal}$ and $q_{e,exp}$, the PO_4^{3-} adsorption by IL-PP is best described by the Elovich equation (R^2 = 0.97, χ^2 = 0.007, $q_{e,cal}$ = 12.11). This kinetic model assumes that the process is controlled by chemisorption and suggests that the adsorbent surface is heterogeneous [64]. The Elovich kinetic model was also postulated by a similar study investigating PO_4^{3-} adsorption on iron hydroxide–eggshell waste [65]. Figure 11 illustrates the experimental kinetics and Elovich fitting model for PO_4^{3-} adsorption by IL-PP.

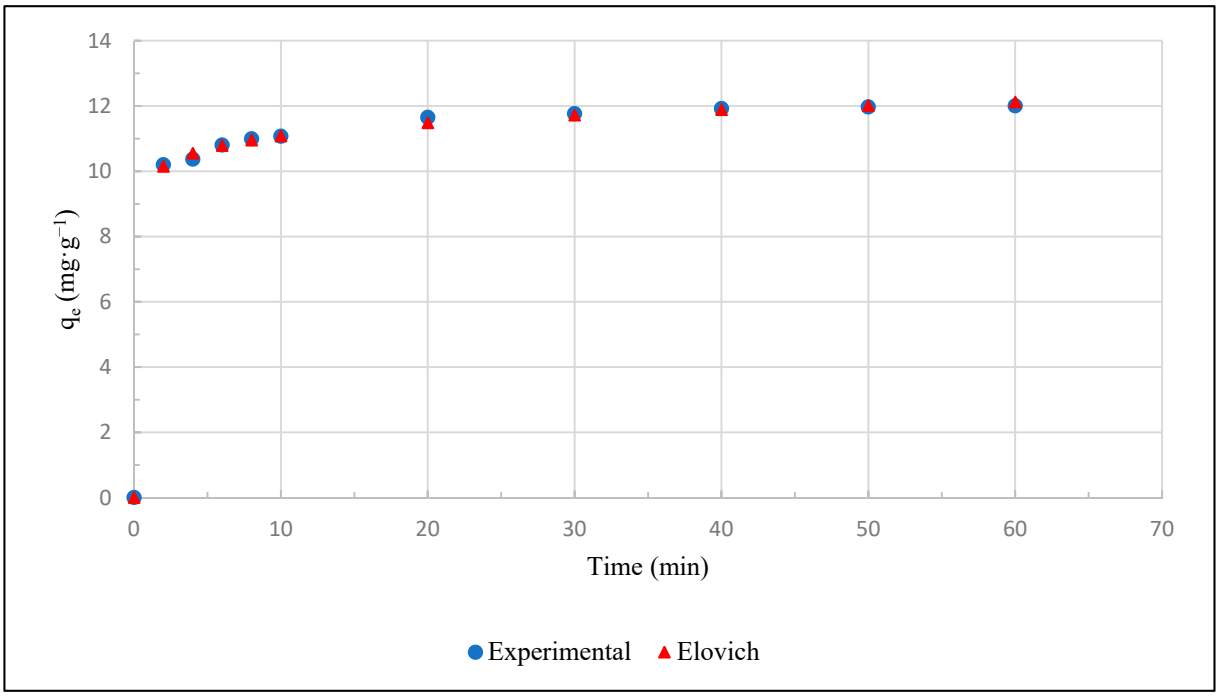

Figure 11. Experimental kinetics and Elovich fitting model for PO_4^{3-} adsorption by IL-PP.

3.3.2. Isotherm

The isotherm is a graph relating q_e to C_e at a constant temperature. Determining the adsorption isotherm helps to describe the adsorbent–adsorbate interaction and thus is indispensable for optimizing the adsorption mechanism pathways, expressing the adsorbent surface properties and capacity, and effectively designing the adsorption system [66]. The Langmuir and Freundlich models were tested to select the isotherm model that adequately describes PO_4^{3-} adsorption by IL-PP. The nonlinear forms of these models are presented in Equations (12) and (13), respectively:

$$q_e = \frac{q_{max}\, K_L C_e}{1 + K_L\, q_e} \tag{12}$$

$$q_e = K_F\, C_e^{\,1/n} \tag{13}$$

where q_e (mg·g^{-1}) is the amount of PO_4-P adsorbed at equilibrium and C_e (mg·L^{-1}) is the PO_4-P concentration in the liquid phase at equilibrium. K_L (L·mg^{-1}) and q_{max} (mg·g^{-1}) are constants of the Langmuir isotherm and indicate the adsorption energy and adsorption density, respectively. K_F and n (dimensionless) are constants of the Freundlich isotherm and indicate the total adsorption capacity and adsorption intensity, respectively. The dimensionless constant R_L presents the separation factor and can be calculated using Equation (14):

$$R_L = \frac{1}{1 + K_L\, c_i} \tag{14}$$

where K_L is the Langmuir equilibrium constant and C_i is the initial PO_4-P concentration. Similar to the kinetic model, the best fitting isotherm model was selected on the basis of the values of R^2 and χ^2.

Table 7 indicates that the PO_4^{3-} adsorption by IL-PP can be described by both the Langmuir (R^2 = 0.98, χ^2 = 0.78) and Freundlich (R^2 = 0.94, χ^2 = 2.62) isotherms, but the former fits better. The Langmuir model assumes that adsorption occurs on a homogenous surface through monolayer coverage. Conversely, the Freundlich model assumes that adsorption occurs on a heterogeneous surface through multilayer coverage and that the adsorbed amount increases with the equilibrium concentration [67].

Table 7. Isotherm models and parameters of PO_4^{3-} adsorption by IL-PP.

Isotherm Model	Parameters	R^2	χ^2
Langmuir	K_L = 0.09 (L·mg^{-1}) q_{max} = 49.12 (mg·g^{-1}) R_L = 0.21	0.98	0.78
Freundlich	K_F = 6.88 1/n = 0.49	0.94	2.62

The suitability of both Langmuir and Freundlich models for describing PO_4^{3-} adsorption by IL-PP suggests that active sites are homogeneously and heterogeneously distributed on the IL-PP surface, so more than one mechanism is involved in the adsorption process [68]. The Langmuir separation factor (R_L = 0.21) is between 0 and 1, and the Freundlich adsorption affinity constant (n = 2.04) is between 1 and 10, which indicates favorable PO_4^{3-} adsorption by IL-PP [58]. Figure 12 shows the experimental isotherm and fitted Langmuir and Freundlich models for PO_4^{3-} adsorption by IL-PP.

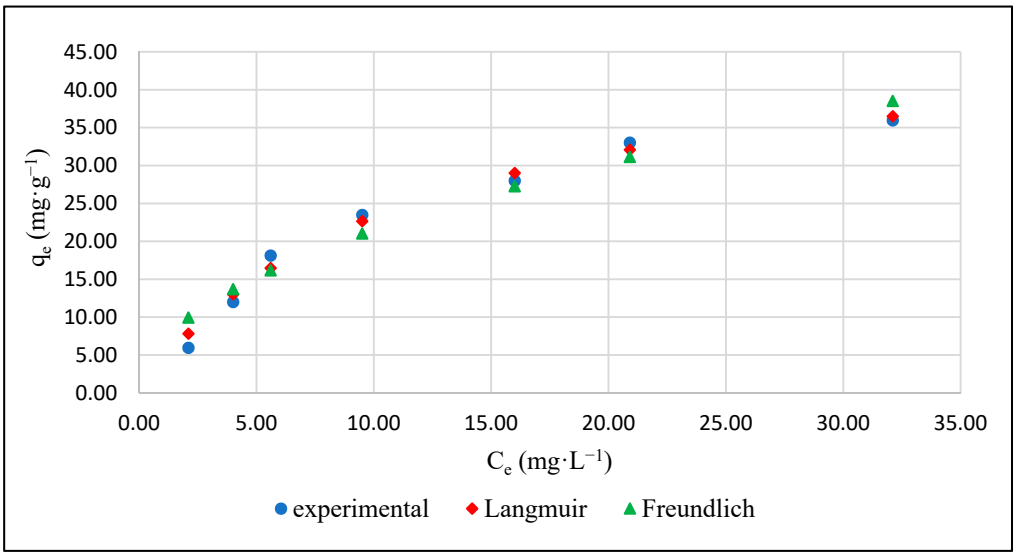

Figure 12. Langmuir and Freundlich isotherms fitted to PO_4^{3-} adsorption by IL-PP.

3.3.3. Thermodynamics

The thermodynamics was studied to determine whether the adsorption process is favorable, spontaneous, exothermic, or endothermic [69]. The change in the Gibbs free energy ΔG was calculated using Equation (5), while ΔH° and ΔS° were calculated from the slope and intercept of the plot of ln K_d versus 1/T using Equation (6), as shown in Figure 13.

Table 8 indicates that the value of ΔG° decreased from −19,836.35 to −22,235.05 J·mol^{-1} when the temperature was increased from 298 to 328 K, which indicates that PO_4^{3-} adsorption by IL-PP was spontaneous and favorable. As the temperature was increased, the process became more spontaneous [70]. The positive ΔH° value (4044.59 J·mol^{-1}) indicates that PO_4^{3-} adsorption by IL-PP is endothermic in nature [71]. The positive ΔS° value (80.04 J·K^{-1}·mol^{-1}) indicates increased randomness at the solid–solution interface and ion replacement during the adsorption process [72].

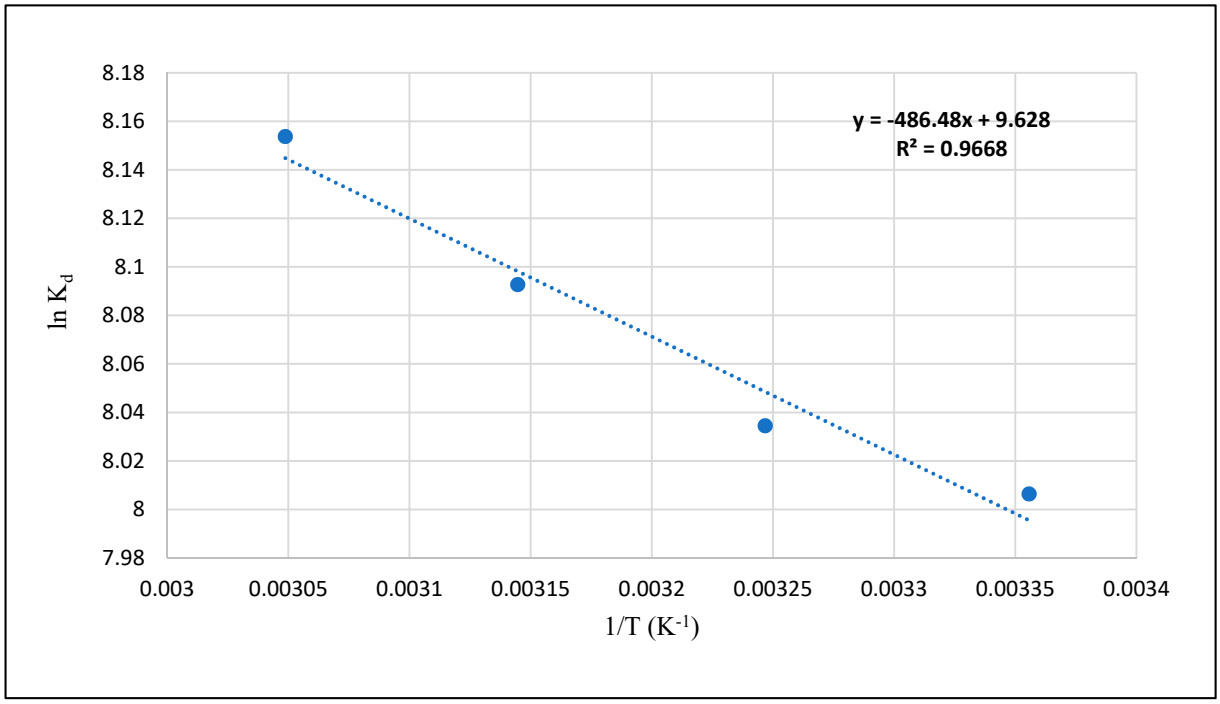

Figure 13. Van 't Hoff plot for PO_4^{3-} adsorption by IL-PP.

Table 8. Thermodynamic parameters of PO_4^{3-} adsorption by IL-PP.

Temperature (K)	ΔG (J·mol^{-1})	ΔH (J·mol^{-1})	ΔS (J·K^{-1}·mol^{-1})
298	−19,836.35	4044.59	80.04
308	−20,573.93		
318	−21,395.71		
328	−22,235.05		

3.3.4. Comparison of IL-PP with Other Iron-Loaded Bio-Adsorbents

Table 9 presents the maximum phosphate adsorption capacity of IL-PP and the most relevant iron-loaded bio-adsorbents. Generally, comparing the performance of bio-adsorbents is complicated because it should take in consideration the adsorption method followed (batch or fixed bed) and working parameters (pH, initial adsorbate concentration, contact time, temperature, adsorbent dose, interfering ions, etc.) [73]. Moreover, a cost-benefit analysis investigating the cost-effectivity, availability and the possibility of reuse is critical for a significant comparison.

Table 9. Basic comparison of IL-PP with most relevant iron-loaded bio-adsorbents.

Bio-Adsorbent	q_{max} (mg PO_4-P/g)	Reference
Fe(III)-loaded orange waste gel	42.72	[74]
Fe(II)-loaded wood particles	17.38	[75]
Fe(II)-loaded sugarcane bagasse	152	[54]
Fe(III)-loaded okara (ILO)	16.66	[43]
Fe(III)-loaded litchi seed waste	100	[76]
Fe(III) impregnated coir pith	70.92	[77]
IL-PP	49.12	This study

4. Conclusions

This study evaluated the efficiency of IL-PP at removing PO_4^{3-} from an aqueous solution. The results indicated that IL-PP is an efficient bio-adsorbent that can be optimized as a green technology for wastewater treatment, waste biomass management, and phosphate

recovery. However, a more detailed study on the performance of IL-PP at removing PO_4^{3-} from real wastewater under real operating conditions is required to check the effect of interfering ions. The successful regeneration and application of phosphate-loaded IL-PP as a fertilizer must also be investigated to make this approach more sustainable and attractive especially in regions known by the huge cultivation of pomegranate fruit.

Author Contributions: Conceptualization, N.B. and C.H.; methodology, N.B. and C.H.; software, N.B.; validation, C.H., S.B. and S.K.; formal analysis, E.T.; investigation, N.B.; resources, B.K. and Z.B.; data curation, N.H. and T.G.; writing—original draft preparation, N.B.; writing—review and editing, C.H.; visualization, A.E.A.; supervision, C.H.; project administration, C.H.; funding acquisition, C.H. All authors have read and agreed to the published version of the manuscript.

Funding: This research received no external funding.

Acknowledgments: Thanks the support of the János Bolyai Research Scholarship of the Hungarian Academy of Sciences (BO/00576/20/4, (BO/00161/21/4) and the New National Excellence Program of the Ministry of Human Capacities UNKP-21-5-550-SZTE).

Conflicts of Interest: The authors declare no conflict of interest.

References

1. Bacelo, H.; Pintor, A.M.A.; Santos, S.C.R.; Boaventura, R.A.R.; Botelho, C.M.S. Performance and prospects of different adsorbents for phosphorus uptake and recovery from water. *Chem. Eng. J.* **2019**, *381*, 122566. [CrossRef]
2. Mayer, B.K.; Baker, L.A.; Boyer, T.H.; Drechsel, P.; Gifford, M.; Hanjra, M.A.; Parameswaran, P.; Stoltzfus, J.; Westerhoff, P.; Rittmann, B.E. Total Value of Phosphorus Recovery. *Environ. Sci. Technol.* **2016**, *50*, 6606–6620. [CrossRef]
3. Melia, P.M.; Cundy, A.B.; Sohi, S.P.; Hooda, P.S.; Busquets, R. Chemosphere Trends in the recovery of phosphorus in bioavailable forms from wastewater. *Chemosphere* **2017**, *186*, 381–395. [CrossRef]
4. Cordell, D.; Rosemarin, A.; Schröder, J.J.; Smit, A.L. Towards global phosphorus security: A systems framework for phosphorus recovery and reuse options. *Chemosphere* **2011**, *84*, 747–758. [CrossRef] [PubMed]
5. Bunce, J.T.; Ndam, E.; Ofiteru, I.D.; Moore, A.; Graham, D.W.; Graham, D.W. A Review of Phosphorus Removal Technologies and Their Applicability to Small-Scale Domestic Wastewater Treatment Systems. *Front. Environ. Sci.* **2018**, *6*, 1–15. [CrossRef]
6. De-Bashan, L.E.; Bashan, Y. Recent advances in removing phosphorus from wastewater and its future use as fertilizer (1997–2003). *Water Res.* **2004**, *38*, 4222–4246. [CrossRef]
7. Sengupta, S.; Nawaz, T.; Beaudry, J. Nitrogen and Phosphorus Recovery from Wastewater. *Curr. Pollut. Rep.* **2015**, *1*, 155–166. [CrossRef]
8. Papargyropoulou, E.; Lozano, R.; Steinberger, J.K.; Wright, N.; Ujang, Z.B. The food waste hierarchy as a framework for the management of food surplus and food waste. *J. Clean. Prod.* **2014**, *76*, 106–115. [CrossRef]
9. Hodúr, C.; Bellahsen, N.; Mikó, E.; Nagypál, V.; Šereš, Z.; Kertész, S. The adsorption of ammonium nitrogen from milking parlor wastewater using pomegranate peel powder for sustainable water, resources, and waste management. *Sustainability* **2020**, *12*, 4880. [CrossRef]
10. Ravindran, R.; Jaiswal, A.K. Exploitation of Food Industry Waste for High-Value Products. *Trends Biotechnol.* **2015**, *34*, 58–69. [CrossRef]
11. Arevalo-gallegos, A.; Ahmad, Z.; Asgher, M.; Parra-saldivar, R.; Iqbal, H.M.N. Sustainable material to produce value-added products with a zero waste approach—A review. *Int. J. Biol. Macromol.* **2017**, *99*, 308–318. [CrossRef]
12. Nguyen, T.A.H.; Ngo, H.H.; Guo, W.; Nguyen, T.V. Phosphorous removal from aqueous solutions by agricultural by-products: A critical review. *J. Water Sustain.* **2012**, *2*, 193–207. [CrossRef]
13. Sulyman, M.; Namiesnik, J.; Gierak, A. Low-cost adsorbents derived from agricultural by-products/wastes for enhancing contaminant uptakes from wastewater: A review. *Pol. J. Environ. Stud.* **2017**, *26*, 479–510. [CrossRef]
14. De Gisi, S.; Lofrano, G.; Grassi, M.; Notarnicola, M. Characteristics and adsorption capacities of low-cost sorbents for wastewater treatment: A review. *Sustain. Mater. Technol.* **2016**, *9*, 10–40. [CrossRef]
15. Yu, F.; Sun, L.; Zhou, Y.; Gao, B.; Gao, W.; Bao, C.; Feng, C. Biosorbents based on agricultural wastes for ionic liquid removal: An approach to agricultural wastes management. *Chemosphere* **2016**, *165*, 94–99. [CrossRef] [PubMed]
16. Solangi, N.H.; Kumar, J.; Mazari, S.A.; Ahmed, S.; Fatima, N.; Mujawar, N.M. Development of fruit waste derived bio-adsorbents for wastewater treatment: A review. *J. Hazard. Mater.* **2021**, *416*, 125848. [CrossRef]
17. Nguyen, T.A.H.; Ngo, H.H.; Guo, W.S.; Zhang, J.; Liang, S.; Lee, D.J.; Nguyen, P.D.; Bui, X.T. Modification of agricultural waste/by-products for enhanced phosphate removal and recovery: Potential and obstacles. *Bioresour. Technol.* **2014**, *169*, 750–762. [CrossRef]
18. Kahramanoglu, I. Trends in Pomegranate Sector: Production, Postharvest Handling and Marketing. *Int. J. Agric. For. Life Sci.* **2019**, *3*, 239–246.

19. Talekar, S.; Patti, A.F.; Vijayraghavan, R.; Arora, A. Complete Utilization of Waste Pomegranate Peels to Produce a Hydrocolloid, Punicalagin Rich Phenolics, and a Hard Carbon Electrode. *ACS Sustain. Chem. Eng.* **2018**, *6*, 16363–16374. [CrossRef]
20. Hadrich, F.; Cherif, S.; Gargouri, Y.T.; Adel, S. Antioxidant and Lipase Inhibitory Activities and Essential Oil Composition of Pomegranate Peel Extracts. *J. Oleo Sci.* **2014**, *63*, 515–525. [CrossRef]
21. Mahdavi, K.; Farhad, A. Application of response surface methodology for the optimization of supercritical fluid extraction of essential oil from pomegranate (*Punica granatum* L.) peel. *J. Food Sci. Technol.* **2016**, *53*, 3113–3121. [CrossRef]
22. Ventura, J.; Alarcón-aguilar, F.; Roman-ramos, R.; Campos-sepulveda, E.; Reyes-vega, M.L.; Boone-villa, V.D.; Jasso-villagómez, E.I.; Aguilar, C.N. Quality and antioxidant properties of a reduced-sugar pomegranate juice jelly with an aqueous extract of pomegranate peels. *Food Chem.* **2013**, *136*, 109–115. [CrossRef]
23. Grabeža, M.; Škrbićb, R.; Stojiljković, M.P.; Rudić-Grujića, V.; Aleksandra, A.; Snježana, P.; Vučić, V.; Mirjanić-Azariće, K.Š.B.; Menković, T.J.N.; Vasiljević, N. Beneficial effects of pomegranate peel extract on plasma lipid profile, fatty acids levels and blood pressure in patients with diabetes mellitus type-2: A randomized, double-blind, placebo-controlled study. *J. Funct. Foods* **2019**, *64*, 103692. [CrossRef]
24. Demiray, E.; Karatay, S.E.; Dönmez, G. Efficient bioethanol production from pomegranate peels by newly isolated Kluyveromyces marxianus. *Energy Sources Part A Recover. Util. Environ. Eff.* **2019**, *42*, 1–10. [CrossRef]
25. Jain, K.; Suryawanshi, P.; Chaudhari, A. Recovery of acerbic anaerobic digester for biogas production from pomegranate shells using organic loading approach. *Indian J. Biochem. Biophys.* **2020**, *57*, 86–94.
26. Ben-Ali, S.; Jaouali, I.; Souissi-Najar, S.; Ouederni, A. Characterization and adsorption capacity of raw pomegranate peel biosorbent for copper removal. *J. Clean. Prod.* **2016**, *142*, 3809–3821. [CrossRef]
27. Ibrahim, T.H.; Gulistan, A.S.; Khamis, M.I.; Ahmed, H.; Aidan, A. Produced water treatment using naturally abundant pomegranate peel. *Desalin. Water Treat.* **2015**, *57*, 1–9. [CrossRef]
28. Turkmen, S.N.; Kipcak, A.S.; Tugrul, N.; Derun, E.M.; Piskin, S. The Adsorption of Zinc Metal in Waste Water Using ZnCl 2 Activated Pomegranate Peel. *Int. J. Mater. Metall. Eng.* **2015**, *9*, 477–480.
29. Khawaja, M.; Shafaq, M.; Kazi, A.A.; Zia-ur-rehman, M.; MuhammadHamid, A. Adsorption studies of pomegranate peel activated charcoal for nickel (II) ion. *J. Chil. Chem. Soc.* **2015**, *60*, 2642–2645. [CrossRef]
30. Alnawab, R.M.; Ridha, A.M. Use of the electrocoagulation with pomegranate peels and zizith's leaves adsorption coupling technique for removal of methylene blue in a batch system. *Int. J. Eng. Technol.* **2018**, *7*, 3451–3458. [CrossRef]
31. Güzel, F.; Aksoy, Ö.; Akkaya, G. Application of Pomegranate (*Punica granatum*) Pulp as a New Biosorbent for the Removal of a Model Basic Dye (Methylene Blue). *World Appl. Sci. J.* **2012**, *20*, 965–975. [CrossRef]
32. Moghadam, M.R.; Nasirizadeh, N.; Dashti, Z.; Babanezhad, E. Removal of Fe (II) from aqueous solution using pomegranate peel carbon: Equilibrium and kinetic studies. *Int. J. Ind. Chem.* **2013**, *4*, 19. [CrossRef]
33. Afsharnia, M.; Saeidi, M.; Zarei, A.; Narooie, M.R.; Biglari, H. Phenol Removal from Aqueous Environment by Adsorption onto Pomegranate Peel Carbon Mojtaba. *Electron. Physician* **2016**, *8*, 3248–3256. [CrossRef]
34. Bellahsen, N.; Varga, G.; Halyag, N.; Kertész, S.; Tombácz, E.; Hodúr, C. Pomegranate peel as a new low-cost adsorbent for ammonium removal. *Int. J. Environ. Sci. Technol.* **2020**, *18*, 711–722. [CrossRef]
35. Bhatnagar, A.; Minocha, A.K. Biosorption optimization of nickel removal from water using Punica granatum peel waste. *Colloids Surf. B Biointerfaces* **2010**, *76*, 544–548. [CrossRef]
36. El-Ashtoukhy, E.S.Z.; Amin, N.K.; Abdelwahab, O. Removal of lead (II) and copper (II) from aqueous solution using pomegranate peel as a new adsorbent. *Desalination* **2008**, *223*, 162–173. [CrossRef]
37. ElNemr, A. Potential of pomegranate husk carbon for Cr(VI) removal from wastewater: Kinetic and isotherm studies. *J. Hazard. Mater.* **2009**, *161*, 132–141. [CrossRef]
38. Senthilkumar, T.; Chattopadhyay, S.K.; Miranda, L.R. Optimization of Activated Carbon Preparation from Pomegranate Peel (*Punica granatum* Peel) Using RSM. *Chem. Eng. Commun.* **2020**, *17*, 238–248. [CrossRef]
39. Ahmad, M.A.; Puad, N.A.A.; Bello, O.S. Kinetic, equilibrium and thermodynamic studies of synthetic dye removal using pomegranate peel activated carbon prepared by microwave-induced KOH activation. *Water Resour. Ind.* **2014**, *6*, 18–35. [CrossRef]
40. Rashtbari, Y.; Hazrati, S.; Afshin, S.; Fazlzadeh, M.; Vosoughi, M. Data on cephalexin removal using powdered activated carbon (PPAC) derived from pomegranate peel. *Data Br.* **2018**, *20*, 1434–1439. [CrossRef]
41. Salmani, M.H.; Abedi, M.; Mozaffari, S.A.; Sadeghian, H.A. Modification of pomegranate waste with iron ions a green composite for removal of Pb from aqueous solution: Equilibrium, thermodynamic and kinetic studies. *AMB Express* **2017**, *7*, 225. [CrossRef]
42. Abdulrazak, Z.N. Pomegranate peel as sorbent in the removal of Pb (II) from wastewater. *J. Eng. Sustain. Dev.* **2016**, *20*, 25–35.
43. Nguyen, T.A.H.; Ngo, H.H.; Guo, W.S.; Zhang, J.; Liang, S.; Tung, K.L. Feasibility of iron loaded "okara" for biosorption of phosphorous in aqueous solutions. *Bioresour. Technol.* **2013**, *150*, 42–49. [CrossRef]
44. Geyikçi, F.; Büyükgüngör, H. Factorial experimental design for adsorption silver ions from water onto montmorillonite. *Acta Geodyn. Geomater.* **2013**, *10*, 363–370. [CrossRef]
45. Tran, H.N.; You, S.J.; Hosseini-Bandegharaei, A.; Chao, H.P. Mistakes and inconsistencies regarding adsorption of contaminants from aqueous solutions: A critical review. *Water Res.* **2017**, *120*, 88–116. [CrossRef]
46. Tran, H.N.; Wang, Y.F.; You, S.J.; Chao, H.P. Insights into the mechanism of cationic dye adsorption on activated charcoal: The importance of Π–Π interactions. *Process Saf. Environ. Prot.* **2017**, *107*, 168–180. [CrossRef]

47. Milonjić, S.K. A consideration of the correct calculation of thermodynamic parameters of adsorption. *J. Serbian Chem. Soc.* **2007**, *72*, 1363–1367. [CrossRef]
48. Savaji, K.V.; Niitsoo, O.; Couzis, A. Influence of particle / solid surface zeta potential on particle adsorption kinetics. *J. Colloid Interface Sci.* **2014**, *431*, 165–175. [CrossRef]
49. Nechifor, G.; Pascu, D.E.; Pascu, M.; Traistaru, G.A.; Bunaciu, A.A.; Aboul-Enein, H.Y. Study of adsorption kinetics and zeta potential of phosphate and nitrate ions on a cellulosic membrane. *Rev. Roum. Chim.* **2013**, *58*, 591–597.
50. Hena, S.; Atikah, S.; Ahmad, H. Removal of phosphate ion from water using chemically modified biomass of sugarcane bagasse. *Int. J. Eng. Sci.* **2015**, *4*, 51–62.
51. Pathak, P.D.; Mandavgane, S.A.; Kulkarni, B.D. Characterizing fruit and vegetable peels as bioadsorbents. *Curr. Sci.* **2016**, *110*, 2114–2115. [CrossRef]
52. Li, M.; Liu, J.; Xu, Y.; Qian, G. Phosphate adsorption on metal oxides and metal hydroxides: A comparative review. *Environ. Rev.* **2016**, *24*, 319–332. [CrossRef]
53. Lǔ, J.; Liu, H.; Liu, R.; Zhao, X.; Sun, L.; Qu, J. Adsorptive removal of phosphate by a nanostructured Fe—Al—Mn trimetal oxide adsorbent. *Powder Technol.* **2013**, *233*, 146–154. [CrossRef]
54. Carvalho, W.S.; Martins, D.F.; Gomes, F.R.; Leite, I.R.; da Silva, L.G.; Ruggiero, R.; Richter, E.M. Phosphate adsorption on chemically modified sugarcane bagasse fibres. *Biomass Bioenergy* **2011**, *35*, 3913–3919. [CrossRef]
55. Worch, E. *Adsorption Technology in Water Treatment: Fundamentals, Processes, and Modeling*; De Gruyter, Hubert & Co. GmbH & Co. KG: Berlin, Germany, 2012.
56. Liu, R.; Chi, L.; Wang, X.; Sui, Y.; Wang, Y.; Arandiyan, H. Review of metal (hydr)oxide and other adsorptive materials for phosphate removal from water. *J. Environ. Chem. Eng.* **2018**, *6*, 5269–5286. [CrossRef]
57. De Sousa, A.F.; Braga, T.P.; Gomes, E.C.C.; Valentini, A.; Longhinotti, E. Adsorption of phosphate using mesoporous spheres containing iron and aluminum oxide. *Chem. Eng. J.* **2012**, *210*, 143–149. [CrossRef]
58. Zhang, B.; Chen, N.; Feng, C.; Zhang, Z. Adsorption for phosphate by crosslinked/non-crosslinked-chitosan-Fe(III) complex sorbents: Characteristic and mechanism. *Chem. Eng. J.* **2018**, *353*, 361–372. [CrossRef]
59. Özbay, N.; Yarg, A.F.J.; Yarbay, R.Z.F.; Önal, E. Full Factorial Experimental Design Analysis of Reactive Dye Removal by Carbon Adsorption. *J. Chem.* **2013**, *2013*, 1–13. [CrossRef]
60. Mekonnen, D.T.; Alemayehu, E.; Lennartz, B. Removal of phosphate ions from aqueous solutions by adsorption onto leftover coal. *Water* **2020**, *12*, 1381. [CrossRef]
61. Hegazy, A.K.; Abdel-Ghani, N.T.; El-Chaghaby, G.A. Adsorption of phenol onto activated carbon from Rhazya stricta: Determination of the optimal experimental parameters using factorial design. *Appl. Water Sci.* **2013**, *4*, 273–281. [CrossRef]
62. Mtaallah, S.; Marzouk, I.; Hamrouni, B. Factorial experimental design applied to adsorption of cadmium on activated alumina Salma Mtaallah, Ikhlass Marzouk and Béchir Hamrouni. *J. Water Reuse Desalination* **2018**, *8*, 76–85. [CrossRef]
63. Regti, A.; el Kassimi, A.; Laamari, M.R.; el Haddad, M. Competitive adsorption and optimization of binary mixture of textile dyes: A factorial design analysis. *J. Assoc. Arab Univ. Basic Appl. Sci.* **2017**, *24*, 1–9. [CrossRef]
64. Tan, K.L.; Hameed, B.H. Insight into the adsorption kinetics models for the removal of contaminants from aqueous solutions. *J. Taiwan Inst. Chem. Eng.* **2017**, *74*, 25–48. [CrossRef]
65. Mezenner, N.Y.; Bensmaili, A. Kinetics and thermodynamic study of phosphate adsorption on iron hydroxide-eggshell waste. *Chem. Eng. J.* **2009**, *147*, 87–96. [CrossRef]
66. Foo, K.Y.; Hameed, B.H. Insights into the modeling of adsorption isotherm systems. *Chem. Eng. J.* **2010**, *156*, 2–10. [CrossRef]
67. Ayawei, N.; Ebelegi, A.N.; Wankasi, D. Modelling and Interpretation of Adsorption Isotherms. *J. Chem.* **2017**, *2017*, 1–11. [CrossRef]
68. Rathod, M.; Mody, K.; Basha, S. Efficient removal of phosphate from aqueous solutions by red seaweed, Kappaphycus alverezii. *J. Clean. Prod.* **2014**, *84*, 484–493. [CrossRef]
69. Doke, K.M.; Khan, E.M. Adsorption thermodynamics to clean up wastewater; critical review. *Rev. Environ. Sci. Biotechnol.* **2013**, *12*, 25–44. [CrossRef]
70. Peng, F.; He, P.W.; Luo, Y.; Lu, X.; Liang, Y.; Fu, J. Adsorption of Phosphate by Biomass Char Deriving from Fast Pyrolysis of Biomass Waste. *Clean—Soil Air Water* **2012**, *40*, 493–498. [CrossRef]
71. Benyoucef, S.; Amrani, M. Adsorption of phosphate ions onto low cost Aleppo pine adsorbent. *Desalination* **2011**, *275*, 231–236. [CrossRef]
72. Liu, Y.; Liu, Y. Biosorption isotherms, kinetics and thermodynamics. *Sep. Purif. Technol.* **2008**, *61*, 229–242. [CrossRef]
73. Loganathan, P.; Vigneswaran, S.; Kandasamy, J.; Nanthi, S. Critical Reviews in Environmental Science: Removal and recovery of phosphate from water using. *Crit. Rev. Environ. Sci. Technol.* **2013**, *44*, 37–41. [CrossRef]
74. Biswas, B.K.; Inoue, K.; Ghimire, K.N.; Ohta, S.; Harada, H.; Ohto, K.; Kawakita, H. The adsorption of phosphate from an aquatic environment using metal-loaded orange waste. *J. Colloid Interface Sci.* **2007**, *312*, 214–223. [CrossRef] [PubMed]
75. Eberhardt, T.L.; Min, S. Biosorbents prepared from wood particles treated with anionic polymer and iron salt: Effect of particle size on phosphate adsorption. *Bioresour. Technol.* **2008**, *99*, 626–630. [CrossRef] [PubMed]

76. Shrestha, A.; Poudel, B.R.; Silwal, M.; Pokhrel, M.R.; Campus, T.M. Adsorptive removal of phosphate onto iron loaded litchi chinensis. *J. Inst. Sci. Technol.* **2018**, *23*, 81–87. [CrossRef]
77. Krishnan, K.A.; Haridas, A. Removal of phosphate from aqueous solutions and sewage using natural and surface modified coir pith. *J. Hazard. Mater.* **2008**, *152*, 527–535. [CrossRef] [PubMed]